

Article

Evaluation of the Performance of a Heat Pipe for Pre-Frozen Soil around a Solar Support by a Numerical Method

Dong Li ¹, Xinpeng Yang ¹, Xuefeng Zhao ^{2,*}, Ruitong Yang ^{1,*}, Lan Meng ² and Shaojie Fu ³

¹ School of Architecture and Civil Engineering, Northeast Petroleum University, Fazhan Lu Street, Daqing 163318, China

² Daqing Oilfield Co., Ltd., Zhongyuan Lu Street, Daqing 163712, China

³ Qinghai Huanghe Photovoltaic System Design Consulting Co., Ltd., Kunlundong Lu Street, Xining 810000, China

* Correspondence: zhaoxuefeng@petrochina.com.cn (X.Z.); yangruitong17@163.com (R.Y.)

Abstract: The base of solar collector systems is usually installed in soil that contains moisture. In cold regions, due to the low ambient temperature, the moisture in the soil freezes, creating a risk of frost heave. This study analyzed the frost heave mechanism of power transmission and transformation foundation, clarified the factors affecting soil frost heave and the way to solve soil layer frost heave, and proposed the use of heat transfer elements to pre-frozen soil layers to prevent the foundation of the solar collector system from freezing. A numerical model of the ground heat exchange pipes in soil was established. The effects of different soil types, soil moisture content, and the effective radius and operating time on the heat transfer performance of the system were investigated by the verified numerical model. The results show that the heat pipe pre-freezing technology can reduce the drop in soil temperature, thereby increasing the temperature difference between the ground heat exchange pipe and the far-field soil. In terms of the ability to delay the decline in soil temperature, reducing the water content and selecting certain clays can increase the degree and speed of the drop in soil temperature.

Keywords: frozen soil; heat pipe; heat transfer; porous media



Citation: Li, D.; Yang, X.; Zhao, X.; Yang, R.; Meng, L.; Fu, S. Evaluation of the Performance of a Heat Pipe for Pre-Frozen Soil around a Solar Support by a Numerical Method. *Processes* **2023**, *11*, 51. <https://doi.org/10.3390/pr11010051>

Academic Editor: Alfredo Iranzo

Received: 30 November 2022

Revised: 21 December 2022

Accepted: 22 December 2022

Published: 26 December 2022



Copyright: © 2022 by the authors. Licensee MDPI, Basel, Switzerland. This article is an open access article distributed under the terms and conditions of the Creative Commons Attribution (CC BY) license (<https://creativecommons.org/licenses/by/4.0/>).

1. Introduction

With the rapid development of the economy and society, the energy problem is increasingly apparent [1,2]. As a new green energy, solar energy has been widely used in various fields [3–5]. However, the pile foundation of solar collectors is affected by frost heaving, which limits its development in cold regions. Especially in northeast China, a significant portion of the soil is seasonally frozen soil. Ground surface soil has continually frozen and thawed due to climate change, and the buried bracket of solar collectors can be damaged by frozen soil during cold climates [6,7]. The continuously repeated deformation of the solar bracket can shorten the running life, but it can also affect the stability of the solar collector system [8,9].

Heat pipe technology is an efficient heat transfer method that can transfer heat over long distances with minimal heat loss. When the heat pipe is buried in the foundation, cold energy is brought into the unfrozen soil, and a frozen area is formed around the heat pipe by using the solidification of the working medium in the soil [10]. Forming a freezing zone and maintaining a certain freezing strength can effectively cut off the passage of rising water and can achieve the purpose of eliminating the destructive effect of soil frost heave in the foundation [11]. Zheng et al. [12] established a numerical model to simulate ground deformation during the construction of the artificial freezing method and verified the effectiveness of the model by comparing the calculation results with the experimental data. Hu et al. [13] advanced a novel antifreeze heating method, using a ground source heat pump to provide heat to reduce the freezing damage of embankments in frigid regions.

The results showed that roadbed frost heave could be quickly dealt with by deploying a direct expansion embankment ground source heat pump to heat the roadbed, with the influence radius being 0.87 m on the first day and 2.03 m on the fifth day. According to the on-site monitoring data, Tian et al. [14] revealed that the subgrade settlement was mainly caused by the melting and consolidation of warm permafrost. To guarantee the standing thermal stability of the embankment and to alleviate the uneven settlement of the pavement, inclined heat pipes should be installed under the subgrade. Gao et al. [15] developed a three-dimensional coupled heat transfer model of the two-phase closed thermal siphon to analyze the heating function of a two-phase closed thermosyphon of the embankment at the seasonal permafrost area of the high-speed railway. The results showed that heating two-phase closed thermosyphons could effectively adjust and improve the ground temperature of the embankment, and the frozen soil depth of the base course was reduced by 1.48 m. Vitel et al. [16] developed an artificial freezing method numerical model to couple the frozen pipe with the surrounding soil, without requiring external temperature or pipe wall flux data to predict surface temperature evolution. Huang et al. [9] presented an improved method for the layout of frozen pipes, which optimized the position of frozen pipes around the circular tunnel. After optimization of the model, the freezing time of pipes was reduced by 70 days. Qi et al. [17] investigated an artificial freezing test to study the thermal state and frost heave law during the freezing process under seepage. The results indicated that frost heave increased with the increase in seepage velocity in the freezing range. Na et al. [18] proposed a stable thermal-hydro-mechanical model to study the phase transition of frozen porous media under finite deformation. The model-simulated consolidation was caused by thawing under geometrical nonlinear conditions. Based on the above research studies, the application of heat pipe technology to solve the frost heave of the equipment foundation has achieved satisfactory results [19–21].

Due to the influence of factors such as the heterogeneity of the soil, the coupled heat exchange between the heat pipe and the soil freezing, and the uncertainty of climate change, the thermal analysis of the frost heave process is complicated, but the effect still lacks in-depth investigation [22,23]. Bai et al. [24] presented a two-phase thermomechanical-coupled model to investigate the effects of cooling temperature and water content on water vapor migration and deformation in soil. They found that the critical initial water content appears between 18.71% and 24.03%, that vapor migrates prominently, and that frost heave develops slowly when the initial water content is lower than the critical value. Bai et al. [25] investigated experiments on the frost-heaving characteristics of unsaturated silty clay. They found that during the phase transition process, there was a mixed removal of water and vapor in the soil, and a bit of ice would form at the top of the sample, while isolated ice would form in frozen unsaturated soil with enough liquid water at the edge of the condensation. Lu et al. [26] investigated experimental studies on the variation of water content, hydrothermal boundary, surface temperature, and matric suction under various soil types. The results indicated that different soil types affected the permafrost upper limit, soil temperature, and volume of unfrozen water content. Stuurop et al. [27] studied the theoretical control of different soil types on frozen soil infiltration through a numerical model of frozen soil infiltration, which indicated that the freezing of percolated water especially hindered infiltration. Based on the Mann–Kendall trend analysis, Hurst index, and Sen's slope analysis, Xu et al. [11] investigated the characteristics of the phase transition state of different types of soil in a frigid region, and the results showed that different climates and different soil types had an impact on soil freeze–thaw. Lu et al. [28] conducted experimental studies on the characteristics of freeze–thaw deformation and the various rules of matric suction. The results showed that the freeze–thaw deformation and matric suction had similar variation trends in the freeze–thaw process; however, the change in volume of unfrozen water content had an obvious effect on the suction of the matrix. Zhang et al. [29] investigated the hydrothermal characteristics of frozen heave of saturated silty clay through experimental studies. The results indicated the critical influence of hydrothermal characteristics on the frost heave of saturated silty clay, but

increasing the pressure during the phase change process would slow down the frost heave. Wang et al. [30] investigated open frost heaving tests on various types of soil to analyze the influence of different soil types on soil frost heaving characteristics. They found that the frost heaving coefficient of fine-grained soil had a critical impact on the soil frost heaving coefficient, while that of coarse-grained soil was mainly affected by mud content.

In severe cold areas, the growth of outdoor solar energy infrastructure construction can bring about more engineering problems due to soil frost heave. However, there are few studies about heat pipe pre-frozen soil before frost heave in the aspect of a solar energy thermal utilization system. As a result of frost heave, the solar flat mount deformation is a common phenomenon, which leads to the tilt of the solar flat, the reduction of received solar energy, and even to damage to the mount. Therefore, strengthening the investigation on temperature variations of heat pipe pre-frozen soil is meaningful. In this paper, a simplified two-dimensional porous medium heat transfer model was established to investigate the thermal performance of ground heat exchange pipes on pre-frozen underground soil around the solar mount and the factors including soil water content and soil type. Furthermore, the effects of radial distance and long-term thermal impact on heat pipe pre-frozen soil are also presented, which provide recommendations for the choice of appositeness regions for pre-frost heave technology for solar infrastructure.

2. Method

2.1. Mathematical Model

Heat exchange between a heat pipe and the soil surrounding it is excessively complex and is affected by soil type, soil water content, freezing radial, and operation time. The digital images of the solar collector mount are shown in Figure 1. To address this complex problem, the following assumptions are proposed to predigest the heat transfer process.

1. The water in soil pores is an incompressible fluid, and convective heat transfer is ignored.
2. The soil is considered an isotropic porous medium with pores filled with water, and the volume change of water during phase transition is ignored.
3. The soil particles are rigid, and the thermophysical properties are independent of temperature.
4. The temperature of the heat pipe is constant.



Figure 1. Digital images of solar collector mount (China Photovoltaic and Energy Storage Demonstration Experimental Platform, Daqing Base).

As a preliminary comparative study, to save the high computational cost of the three-dimensional model, a two-dimensional model of the section where the heat pipe is located was carried out. The model only considers the transverse and longitudinal heat transfer, and only the heat transfer process on the plane was studied; therefore, it was solved using the Cartesian coordinate system [15,31]. The changes in medium owing to swelling and erosion are complex processes [32]. To simplify the calculation, the static interface in the pores was assumed. The simplified two-dimensional model is shown in Figure 2. The ground is exposed to the environment, and convection heat is an exchange with the air on

the ground. The buried pipeline conducts heat with the soil and the water in the soil pores. The water in the soil pores starts to solidify and release latent heat as the temperature falls below the melting point of water. The area outside the calculation boundary is not affected by the cooling of underground pipes.

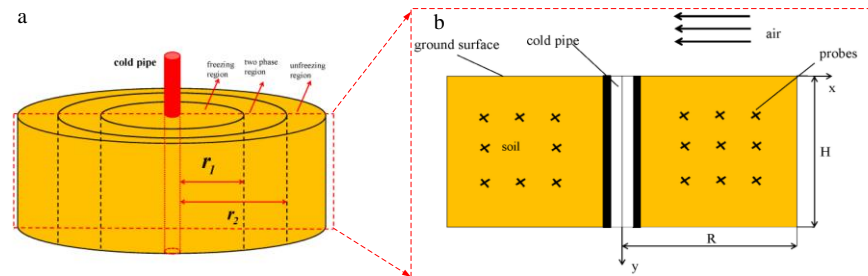


Figure 2. Physical model of underground soil and heat pipe. (a) 3D model; (b) simplified 2D model.

2.2. Governing Equations and Boundary Conditions

As the natural convection of water in probes is neglected, only the energy equation was solved in the present work.

The governing equation can be divided into three computation regions according to phase [33].

The solid region ($T < T_s$),

$$\frac{\partial T}{\partial \tau} (\beta \rho_s c_s + (1 - \beta) \rho_p c_p) = \lambda_{eff} \left(\frac{\partial^2 T}{\partial x^2} + \frac{\partial^2 T}{\partial y^2} \right) \quad (1)$$

The fluid region ($T > T_l$),

$$\frac{\partial T}{\partial \tau} (\beta \rho_l c_l + (1 - \beta) \rho_p c_p) = \lambda_{eff} \left(\frac{\partial^2 T}{\partial x^2} + \frac{\partial^2 T}{\partial y^2} \right) \quad (2)$$

The two-phase region ($T_s < T < T_l$),

$$\frac{\partial T}{\partial \tau} (f \beta \rho_l c_l + (1 - f) \beta \rho_s c_s + (1 - \beta) \rho_p c_p) = \lambda_{eff} \left(\frac{\partial^2 T}{\partial x^2} + \frac{\partial^2 T}{\partial y^2} \right) + \beta L \frac{\partial f}{\partial \tau} \quad (3)$$

$$\lambda_{eff} = \beta (f \lambda_l + (1 - f) \lambda_s) + (1 - \beta) \lambda_p \quad (4)$$

where T is temperature, τ is time, and β is porosity. P , c , and λ represent the density, specific heat capacity, and thermal conductivity, respectively. λ_{eff} stands for the integrated thermal conductivity of the soil. L indicates the latent heat. Meanwhile, the subscripts p , s , and l stand for the soil, and water in solid and liquid, respectively.

L and λ_{eff} represent the latent heat of the water and the average thermal conductivity. F is the liquid phase rate, characterizing the proportion of liquid components in the phase change process of water, which can be defined as [33]:

$$f = \begin{cases} 0 & T < T_s \\ \frac{T - T_s}{T_L - T_s} & T_s < T < T_L \\ 1 & T > T_L \end{cases} \quad (5)$$

where T_s and T_L are the melting temperature and freezing temperature of the water, respectively.

Initial condition:

$$T = T_0(x, y) \quad (6)$$

Boundary conditions:

$$y = 0 - \lambda \left. \frac{\partial T(x, y, \tau)}{\partial y} \right|_{y=0} = h_w (T_a - T(x, y, \tau)|_{y=0}) \quad (7)$$

$$z = H \left. \frac{\partial T(x, y, \tau)}{\partial y} \right|_{y=H} = 0 \quad (8)$$

$$x = d/2 T(x, y, \tau)|_{x=d/2} = T_1 \quad (9)$$

$$x = R \left. \frac{\partial T(x, y, \tau)}{\partial x} \right|_{x=R} = 0 \quad (10)$$

where T_a and T_0 stand for the ambient temperature and the temperature of an outer surface of the heat pipe, respectively. d is the diameter of the heat pipe. h_w represents the comprehensive convective heat transfer coefficient between the ambient and ground surface.

2.3. Solution and Validation of the Model

In the present work, the simulation was differentiated using an implicit format and was solved iteratively with second-order accuracy. The computational region is divided into several finite volumes by the structured mesh of ICEM software. Through the grid independence test, the models with 26,789, 60,300, and 107,065 grids were tested for grid independence. The calculation results are shown in Figure 3a. The calculation results of models with 60,300 and 107,065 grids are consistent, and thus, the model with 60,300 grids was selected for calculation. The generated grid diagram is shown in Figure 3b. FLU-ENT2021 was used to solve the calculation, in which the finite volume method was used to discretize the mathematical equation, and the second-order precision implicit method was used for iterative calculation. To ensure the reliability of the calculation results, the convergence criterion was 10^{-6} . The buried depth of ground heat exchange pipes (GHEPs) was 1 m, while the temperature of the heat pipe was set to 250 K. The air temperature and combined convective heat transfer coefficient of the ground surface were 268 K and 23.2 W/(m·K), respectively. The parameters of the materials are shown in Table 1.

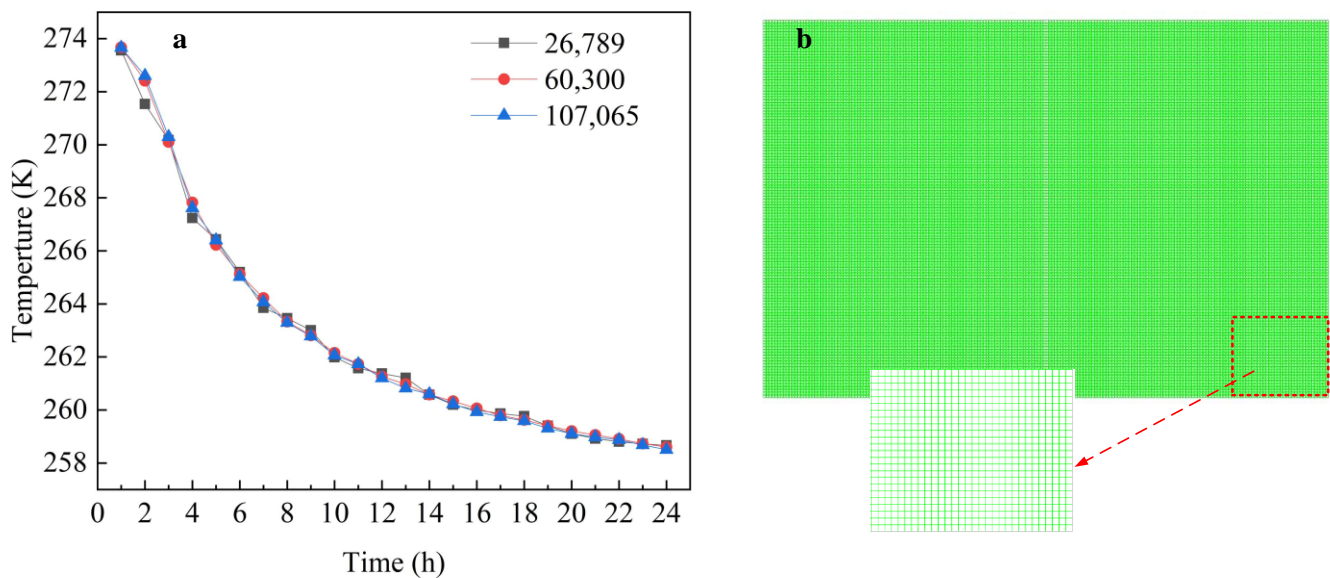


Figure 3. Results of grid independence verification (a) and the generated grid diagram (b).

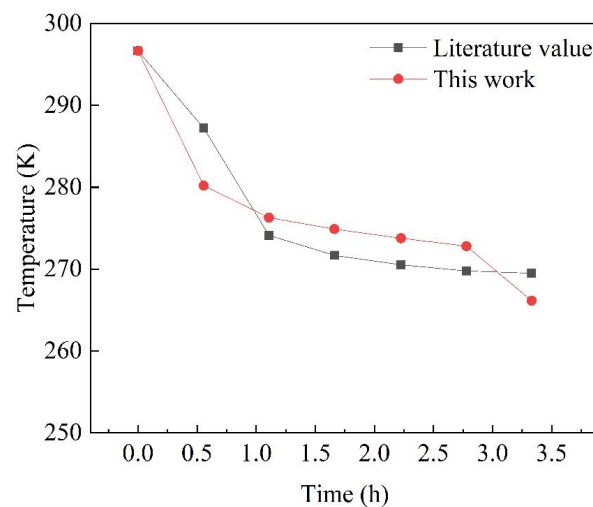
Table 1. Thermal properties of soil matrix and water.

Materials	Density (kg/m ³)	Specific Heat Capacity (J/kg·K)		Thermal Conductivity (W/m·K)		Thermal Diffusivity mm ² /s	Latent Heat (J/kg·K)
Clay	1500	1100		0.9		0.545	-
Sand	1900	1260		1.8		0.752	-
Sandstone	2500	1110		2.5		0.900	-
Soil	1500	1000		2		1.333	-
Water	1000	Liquid	4189	Liquid	0.56	0.131	333,400
		Solid	2093	Solid	2.24	0.143	

The numerical procedure for heat transfer of GHEPs was compared with the experimental results in the published literature [34] to verify the accuracy and reliability of the numerical solution. In the reference, the temperature of GHEPs is 254.45 K, and the initial temperature of the soil is 296.65 K. The physical parameters of the soil are shown in Table 2. The comparison of the soil temperature at 25 mm away from the heat pipe is shown in Figure 4. It can be seen that the numerical results of the soil temperature at 25 mm away from the outer pipe wall are close to the literature data, with an average relative difference of 1.33%, which is acceptable for the current work.

Table 2. Material parameters in the referenced literature [34].

Materials	Density (kg/m ³)	Specific Heat Capacity (J/kg·K)	Thermal Conductivity (W/m·K)	Thermal Diffusivity m ² /day	Porosity
Dry sand	2650	1100	0.29	0.0198	0.36

**Figure 4.** Variability of soil temperature with time.

3. Results and Discussion

Based on the above-established numerical simulation model of frozen soil, the heat transfer performance and soil temperature distribution of water-bearing soil under the operating conditions of GHEP were studied. To characterize the typical freezing phenomenon of the soil heat transfer, the latent heat of water was reduced for calculation. Figure 5 shows the temperature and soil temperature distributions at different locations after GHEP was run for one day. The heat pipe pre-freezing technology can reduce the rate of decreasing soil temperature, thereby maintaining the temperature difference between the heat pipe and the distant soil.

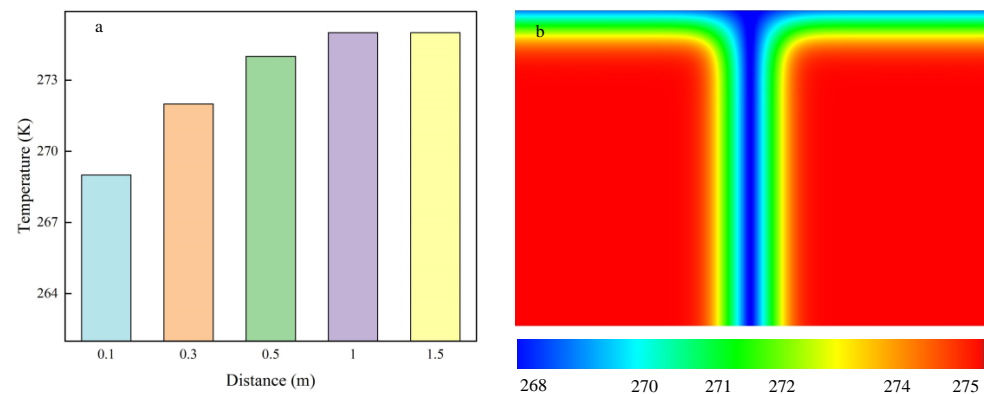


Figure 5. Typical freezing phenomenon characteristics: (a) temperature; (b) temperature distribution.

3.1. Spatiotemporal Characteristics of Soil Freezing

To obtain the spatiotemporal characteristics of soil, the heat transfer of the heat pipe under the condition of soil porosity of 0.25 was investigated. The following figures show the relationship between the GHEP radius of action and operating time. As shown in Figure 6a, the soil temperature at 0.1 m from the buried pipe decreases rapidly within a month, and with the increase in distance from GHEP, the degree of soil temperature decreasing with operation time becomes flat. Once the distance is up to 1 m, the soil temperature is no longer affected by the heat from the GHEP, indicating that the selected GHEP has a maximum influence radius within 1 m in sandy soil. In Figure 6b, the soil liquid fraction versus the distance from the GHEP is plotted. At 0.1 m from the pipe, the fraction gradually decreases until it reaches 0 after operating for 1 day. At 0.3 m from the GHEP, the soil liquid fraction starts to decrease at about two runtimes, and fewer changes in the soil liquid phase rate occur when the pipe is 0.5 m or farther from the GHEP in the first week. As the position becomes closer to the GHEP, the phase state of the water changes dramatically with time. It was found that the liquid fraction is an effective parameter for judging GHEP mitigation of soil freezing, and complete freezing happened only within 0.5 m from the GHEP in soil within 10 days.

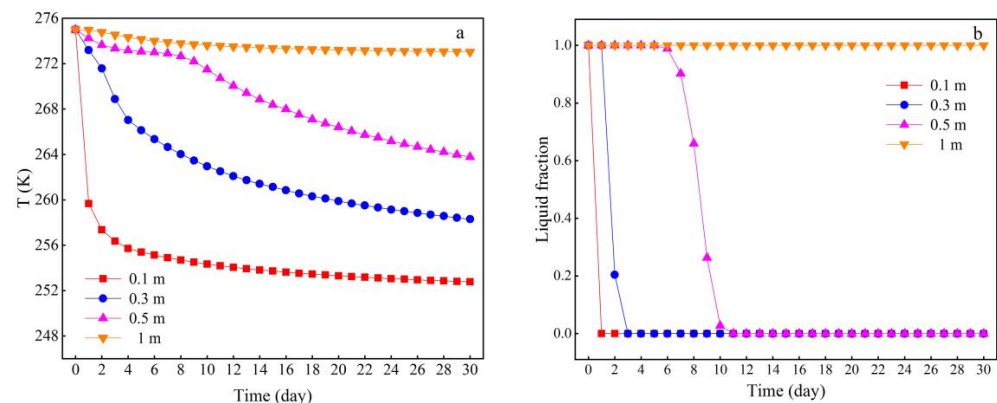


Figure 6. Variation of soil temperature and liquid fraction with radial distance: (a) temperature; (b) liquid fraction.

Figure 7 shows that the soil temperature after one month of operation was 250 K for the freezing region and 275 K for the unfreezing region. Additional analysis reveals that after a week of operation, the temperature of the soil medium near the buried pipe gradually decreases, and an irregular cooling zone appears around the buried pipe, which diffuses over the far field from the boundaries surrounded by the soil. The temperature difference between GHEP and far-field soil is large because of the latent heat released with the water freezing, thereby attenuating the drop in soil temperature. It helps to improve

the heat transfer efficiency of the GHEP, shorten the buried depth of the GHEP, and reduce the initial cost.

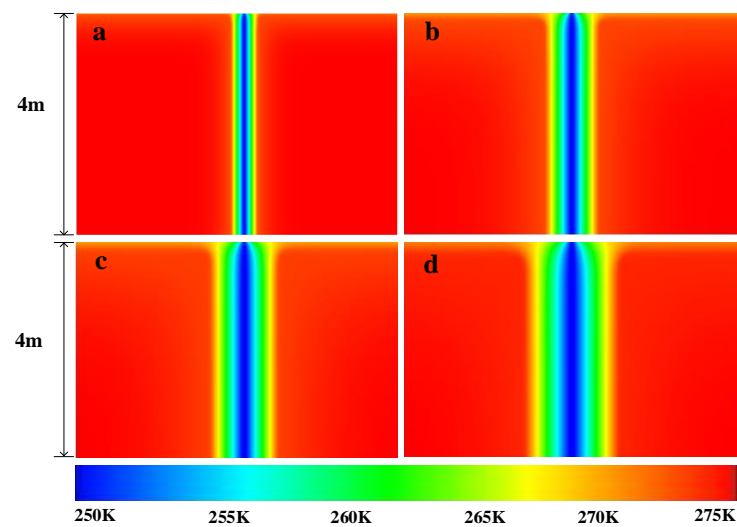


Figure 7. Soil temperature distribution of the calculation region for a month-long operation: (a) after 1 day; (b) after 1 week; (c) after 2 weeks; (d) after 1 month.

3.2. Effects of Soil Moisture Content on Freezing

Soil water content is one of the important parameters of soil frost heave, and Figure 8 shows the influence of soil moisture on the temperature and liquid fraction at the monitoring site during the GHEP operation time. It can be seen from Figure 8a that during the operation of GHEP, the soil temperature gradually declines in a step shape, which is due to the fact that the water in the pores releases latent heat during phase change, making its temperature gradient low. When it is completely solidified, the heat is released as sensible heat, and the temperature drops sharply. The soil temperature increased with the increase in water content during GHEP operation time. This phenomenon is attributed to exothermic water solidification, and the lower the temperature decrease, the higher the soil moisture. A similar conclusion can be demonstrated by the phase transition observed in Figure 8b, where soils with low β respond more quickly to the freezing process. In terms of the freezing process, when the water content is 0.15, the soil starts to freeze first after 1 h of operation until 4 h to complete freezing, and soils with higher β require more thermal power from GHEP. The high water content of the soil is not conducive to GHEP freezing the soil in frigid regions.

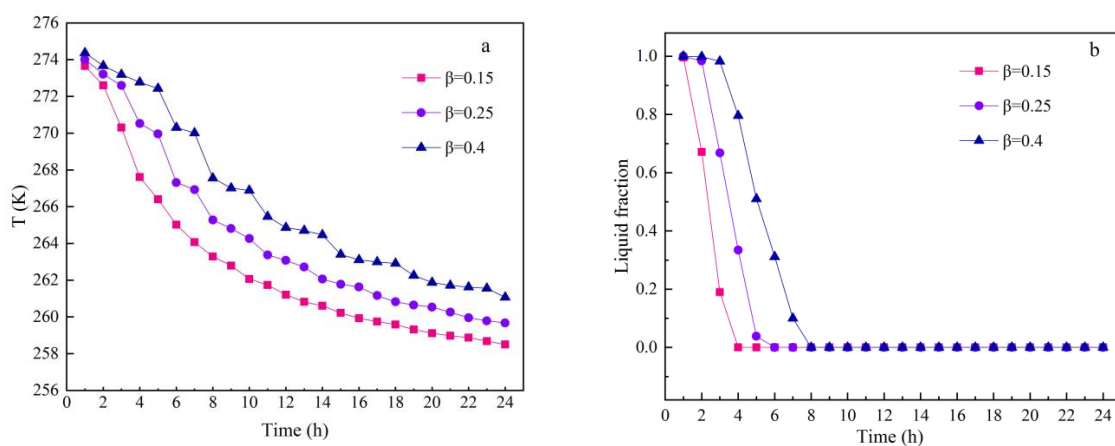


Figure 8. Variation of temperature and liquid fraction with soil porosity versus (a) temperature; (b) liquid fraction.

3.3. Effects of Soil Types on Freezing

In the present work, the freezing properties of different soil types with a porosity of 0.25 were studied. Figure 9a shows the influence of GHEP on the temperature field in different soil types. Based on the figure, temperature changes the most during the same period, followed by sandstone and clay temperature, which change the least. This is primarily due to the disparity in physical properties between different types of soil. It can be seen in Table 1 that clay has the lowest diffusion coefficient and thermal conductivity, resulting in weak heat transfer and small temperature changes. Sand temperatures farther away from the GHEP will drop less rapidly than other soil types due to the lower rate of thermal diffusion.

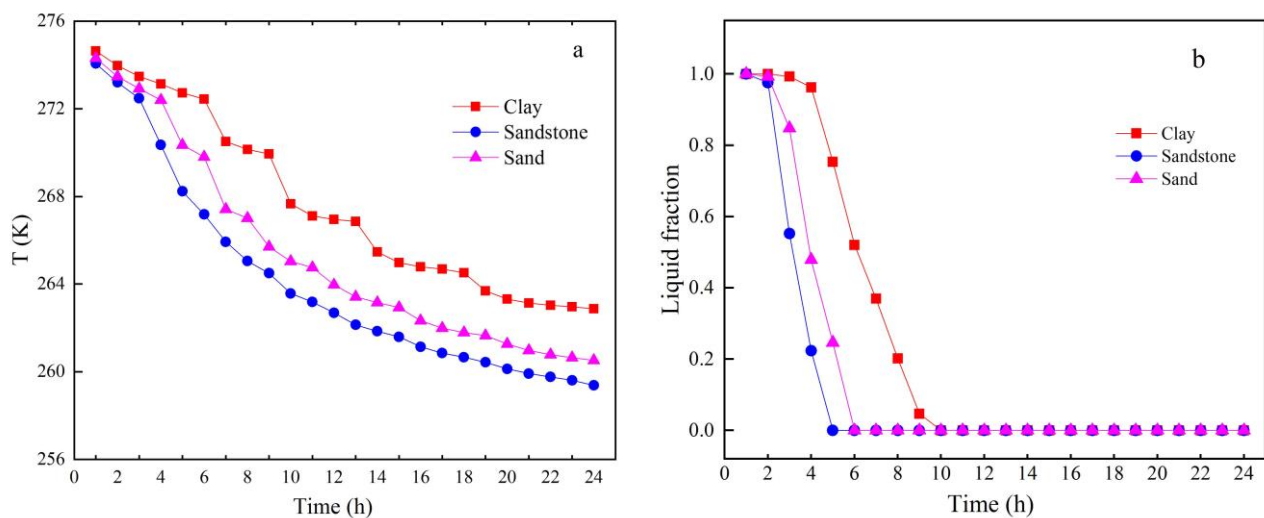


Figure 9. Variation of temperature and liquid fraction with soil types versus (a) temperature; (b) liquid fraction.

Figure 9b indicates the change in the soil liquid fraction with the GHEP cooling time under various soil types. The liquid fraction gradually decreases with the operation time, and the freezing rate has a great dependence on the soil thermal diffusion coefficient, and the degree of the freezing coefficient gradually increases with the decrease in the thermal diffusion coefficient. The reason is that the heat transfer rate of GHEP to the soil will decrease due to the decrease in thermal diffusivity of the soil, and a higher thermal diffusivity will increase the transfer of cold energy of CHEP to the soil. This means that the increase in the soil thermal diffusivity increases the rate of soil temperature drop. Therefore, the more cooling energy absorbed by the water in the soil pores, the faster the solidification, and the higher the liquid phase rate of the water in the pores. Therefore, the freezing ability of sandstone is lower than sand, and the freezing ability of clay is the worst.

4. Conclusions

In the present work, a numerical model was established to simulate and study the heat transfer performance of GHEP to the surrounding porous media with water-bearing soil. The effect of soil type and soil water content on the temperature variation characteristics and spatial-temporal distribution of soil under long-term operation in frigid regions were numerically investigated. The conclusions can be drawn as follows:

- (1) For GHEP with long-term operation, since the water in soil pores can release latent heat during the solidification process, increasing the water content can slow down the rate of soil temperature drop.
- (2) The action radius of GHEP is limited. The studied GHEP can unfreeze the pre-frozen soil within a radius of 0.5 m within one month of operation.
- (3) Increasing soil water content is not conducive to the heat transfer of GHEP to the surrounding soil in frigid regions. The higher the soil moisture content, the warmer

the surrounding of the GHEP is, and thus, the more thermal power that is required. The pre-frozen technology is more suitable for soil with low water content.

(4) The solidification rate of water in soil pores is mainly affected by the thermal diffusivity of the soil. Among the three soil types studied, sandstone was the best, and clay was the worst in terms of their ability to accelerate the drop in soil temperature.

Author Contributions: D.L.: data curation; methodology; validation; writing—original draft. X.Y.: formal analysis; software; writing—original draft. X.Z. data curation; validation; writing—original draft; writing—review and editing. R.Y.: formal analysis; methodology; software; writing—review and editing. L.M.: software; supervision. S.F.: methodology. All authors have read and agreed to the published version of the manuscript.

Funding: This research was funded by the Scientific and Technological Object of Daqing city, China, grant number No. HGS-KJ/KJGLB- [2021] No30.

Institutional Review Board Statement: Not applicable.

Informed Consent Statement: Not applicable.

Data Availability Statement: The datasets used and/or analyzed during the current study are available from the corresponding authors upon reasonable request.

Conflicts of Interest: The authors declare that they have no known competing financial interest or personal relationships that could have appeared to influence the work reported in this paper.

References

- Guler, E.; Kandemir, S.Y.; Acikkalp, E.; Ahmadi, M.H. Evaluation of sustainable energy performance for OECD countries. *Energy Sources Part B Econ. Plan. Policy* **2021**, *16*, 491–514. [[CrossRef](#)]
- Açikkalp, E.; Kandemir, S.Y. A method for determining optimum insulation thickness: Combined economic and environmental method. *Therm. Sci. Eng. Prog.* **2019**, *11*, 249–253. [[CrossRef](#)]
- Açikkalp, E.; Kandemir, S.Y.; Ahmadi, M.H. Solar driven Stirling engine—Chemical heat pump—Absorption refrigerator hybrid system as environmental friendly energy system. *J. Environ. Manag.* **2019**, *232*, 455–461. [[CrossRef](#)] [[PubMed](#)]
- Hassan, A.A.; Elwardany, A.E.; Ookawara, S.; El-Sharkawy, I.I. Performance investigation of a solar-powered adsorption-based trigeneration system for cooling, electricity, and domestic hot water production. *Appl. Therm. Eng.* **2021**, *199*, 117553. [[CrossRef](#)]
- Jiang, B.; Lougou, B.G.; Zhang, H.; Wang, W.; Han, D.; Shuai, Y. Analysis of high-flux solar irradiation distribution characteristic for solar thermochemical energy storage application. *Appl. Therm. Eng.* **2020**, *181*, 115900. [[CrossRef](#)]
- Shan, W.; Zhang, C.; Guo, Y.; Qiu, L.; Xu, Z.; Wang, Y. Spatial Distribution and Variation Characteristics of Permafrost Temperature in Northeast China. *Sustainability* **2022**, *14*, 8178. [[CrossRef](#)]
- Ding, F.; Song, L.; Yue, F. Study on Mechanical Properties of Cement-Improved Frozen Soil under Uniaxial Compression Based on Discrete Element Method. *Processes* **2022**, *10*, 324. [[CrossRef](#)]
- Huang, S.; Guo, Y.; Liu, Y.; Ke, L.; Liu, G.; Chen, C. Study on the influence of water flow on temperature around freeze pipes and its distribution optimization during artificial ground freezing. *Appl. Therm. Eng.* **2018**, *135*, 435–445. [[CrossRef](#)]
- Zhang, Q.; Song, Z.; Li, X.; Wang, J.; Liu, L. Deformation behaviors and meso-structure characteristics variation of the weathered soil of Pisha sandstone caused by freezing–thawing effect. *Cold Reg. Sci. Technol.* **2019**, *167*, 102864. [[CrossRef](#)]
- Duan, Y.; Rong, C.; Cheng, H.; Cai, H.; Wang, Z.; Yao, Z. Experimental and Numerical Investigation on Improved Design for Profiled Freezing-tube of FSPR. *Processes* **2020**, *8*, 992. [[CrossRef](#)]
- Xu, S.; Fu, Q.; Li, T.; Meng, F.; Liu, D.; Hou, R.; Li, M.; Li, Q. Spatiotemporal characteristics of the soil freeze-thaw state and its variation under different land use types—A case study in Northeast China. *Agric. For. Meteorol.* **2022**, *312*, 108737. [[CrossRef](#)]
- Zheng, L.; Gao, Y.; Zhou, Y.; Liu, T.; Tian, S. A practical method for predicting ground surface deformation induced by the artificial ground freezing method. *Comput. Geotech.* **2021**, *130*, 103925. [[CrossRef](#)]
- Hu, T.; Liu, J.; Yue, Z.; Xu, L.; Zhang, Z. Proposed application of a geothermal heat pump technique to address frost damage of embankments in cold regions. *Cold Reg. Sci. Technol.* **2022**, *195*, 103474. [[CrossRef](#)]
- Tian, Y.; Yang, Z.; Liu, Y.; Cai, X.; Shen, Y. Long-term thermal stability and settlement of heat pipe-protected highway embankment in warm permafrost regions. *Eng. Geol.* **2021**, *292*, 106269. [[CrossRef](#)]
- Gao, J.; Lai, Y.; Zhang, M.; Chang, D. The thermal effect of heating two-phase closed thermosyphons on the high-speed railway embankment in seasonally frozen regions. *Appl. Therm. Eng.* **2018**, *141*, 948–957. [[CrossRef](#)]
- Vitel, M.; Rouabhi, A.; Tijani, M.; Guérin, F. Modeling heat transfer between a freeze pipe and the surrounding ground during artificial ground freezing activities. *Comput. Geotech.* **2015**, *63*, 99–111. [[CrossRef](#)]
- Qi, J.; Wang, F.; Peng, L.; Qu, Y.; Zhao, J.; Liang, J. Model test on the development of thermal regime and frost heave of a gravelly soil under seepage during artificial freezing. *Cold Reg. Sci. Technol.* **2022**, *196*, 103495. [[CrossRef](#)]

18. Na, S.; Sun, W. Computational thermo-hydro-mechanics for multiphase freezing and thawing porous media in the finite deformation range. *Comput. Methods Appl. Mech. Eng.* **2017**, *318*, 667–700. [[CrossRef](#)]
19. Huang, X.; Rudolph, D.L. A hybrid analytical-numerical technique for solving soil temperature during the freezing process. *Adv. Water Resour.* **2022**, *162*, 104163. [[CrossRef](#)]
20. Wu, Y.; Zhai, E.; Zhang, X.; Wang, G.; Lu, Y. A study on frost heave and thaw settlement of soil subjected to cyclic freeze-thaw conditions based on hydro-thermal-mechanical coupling analysis. *Cold Reg. Sci. Technol.* **2021**, *188*, 103296. [[CrossRef](#)]
21. Wang, T.; Liu, Y.; Zhou, G.; Wang, D. Effect of uncertain hydrothermal properties and freezing temperature on the thermal process of frozen soil around a single freezing pipe. *Int. Commun. Heat Mass Transf.* **2021**, *124*, 105267. [[CrossRef](#)]
22. Zhang, M.; Lu, J.; Pei, W.; Lai, Y.; Yan, Z.; Wan, X. Laboratory study on the frost-proof performance of a novel embankment dam in seasonally frozen regions. *J. Hydrol.* **2021**, *602*, 126769. [[CrossRef](#)]
23. Zhang, X.; Wu, Y.; Zhai, E.; Ye, P. Coupling analysis of the heat-water dynamics and frozen depth in a seasonally frozen zone. *J. Hydrol.* **2021**, *593*, 125603. [[CrossRef](#)]
24. Bai, R.; Lai, Y.; Zhang, M.; Ren, J. Study on the coupled heat-water-vapor-mechanics process of unsaturated soils. *J. Hydrol.* **2020**, *585*, 124784. [[CrossRef](#)]
25. Bai, R.; Lai, Y.; Pei, W.; Zhang, M. Study on the frost heave behavior of the freezing unsaturated silty clay. *Cold Reg. Sci. Technol.* **2022**, *197*, 103525. [[CrossRef](#)]
26. Lu, J.; Zhang, M.; Pei, W. Hydro-thermal behaviors of the ground under different surfaces in the Qinghai-Tibet Plateau. *Cold Reg. Sci. Technol.* **2019**, *161*, 99–106. [[CrossRef](#)]
27. Stuurop, J.C.; van der Zee, S.E.; French, H.K. The influence of soil texture and environmental conditions on frozen soil infiltration: A numerical investigation. *Cold Reg. Sci. Technol.* **2022**, *194*, 103456. [[CrossRef](#)]
28. Lu, J.; Zhang, M.; Zhang, X.; Pei, W.; Bi, J. Experimental study on the freezing–thawing deformation of a silty clay. *Cold Reg. Sci. Technol.* **2018**, *151*, 19–27. [[CrossRef](#)]
29. Zhang, X.; Zhang, M.; Lu, J.; Pei, W.; Yan, Z. Effect of hydro-thermal behavior on the frost heave of a saturated silty clay under different applied pressures. *Appl. Therm. Eng.* **2017**, *117*, 462–467. [[CrossRef](#)]
30. Wang, W.; Zhang, X.; Lü, Y. An open frozen–heave test on the pipeline foundation soils in the permafrost regions. *Nat. Gas Ind. B* **2018**, *5*, 219–225. [[CrossRef](#)]
31. Sun, W.; Cheng, Q.; Zheng, A.; Gan, Y.; Gao, W.; Liu, Y. Heat flow coupling characteristics analysis and heating effect evaluation study of crude oil in the storage tank different structure coil heating processes. *Int. J. Heat Mass Transf.* **2018**, *127*, 89–101. [[CrossRef](#)]
32. ANSYS. *ANSYS Fluent Technical Staff, ANSYS Fluent 2021; Users Guide*; ANSYS, Inc.: Canonsburg, PA, USA, 2021.
33. Matias, A.F.; Coelho, R.C.; Andrade, J.S.; Araújo, N.A. Flow through time–evolving porous media: Swelling and erosion. *J. Comput. Sci.* **2021**, *53*, 101360. [[CrossRef](#)]
34. Eslami-Nejad, P.; Bernier, M. Freezing of geothermal borehole surroundings: A numerical and experimental assessment with applications. *Appl. Energy* **2012**, *98*, 333–345. [[CrossRef](#)]

Disclaimer/Publisher’s Note: The statements, opinions and data contained in all publications are solely those of the individual author(s) and contributor(s) and not of MDPI and/or the editor(s). MDPI and/or the editor(s) disclaim responsibility for any injury to people or property resulting from any ideas, methods, instructions or products referred to in the content.